# Active Huygens' Metasurfaces for RF Waveform Synthesis in a Cavity

Alex M. H. Wong

Rogers S. Sr. Department of
Electrical and Computer Engineering
University of Toronto
Toronto, Canada M5S 3G4
Email: alex.wong@mail.utoronto.ca

George V. Eleftheriades

Rogers S. Sr. Department of
Electrical and Computer Engineering
University of Toronto
Toronto, Canada M5S 3G4
Email: gelefth@ece.utoronto.ca

*Abstract*—Metasurfaces are engineered surfaces which exhibit unconventional electromagnetic properties. Various recent proposals of metasurfaces — many of which are constructed with micro- and nano- circuit elements — explore possible applications including arbitrary reflection, transmission, focusing, collimation, and polarization operations on incident electromagnetic waves. However, possible applications for active and non-planar metasurfaces remain largely unexplored.

In this work we report our study on active Huygens' metasurfaces which completely enclose an area. We report the theoretical groundwork, describe the metasurface element and system design, then showcase simulation and experimental results in generating an arbitrary waveform within a closed area using the proposed active closed Huygens' surfaces. The proliferation of such surfaces will find applications in medical imaging and therapy, power concentration and electromagnetic characterization.

## I. INTRODUCTION

Metamaterials — artificial materials with electromagnetic properties unmatched in nature — provide new and exciting possibilities for the manipulation of electromagnetic waves [1]. A type of metamaterials called transmission-line metamaterials (TLMs) [2] are of specific interest to electrical engineers, as they use electrical circuit components to tailor the electromagnetic effect of materials, and achieve useful or exotic material effects, such as negative refractive index and extreme anisotropy. The TLM represents a circuit-based paradigm for analyzing and designing metamaterials and metasurfaces [3] — 2D equivalents of metamaterials. The developments of metasurfaces has received much recent interest due to their relative simplicity compared to their 3D counterparts, which in most cases lead to reduced fabrication requirement and cost.

In this regard, novel arrangements of 2D RF circuitry have been employed to build metasurfaces which perform anomalous refraction, arbitrary reflection, near-field and far-field focusing and polarization conversion [4]–[11]. Circuit analogies have also been carried to optical regimes: it has been established that one can efficiently analyze the electromagnetic response of plasmonic and dielectric materials using circuit analogies [12]. Through this analogy, optical circuit elements and antennas have been successfully employed in metasurfaces which perform many of the aforementioned operations, to varying degrees of effectiveness [13]–[19]. However, while a plethora of proposals have emerged regarding passive planar metasurfaces, the extended realm of possibilities for active
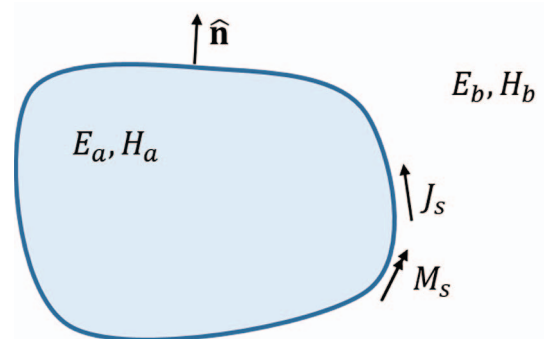


Fig. 1. A diagram illustrating the equivalence principle for electromagnetic waves. Subscripts $a$ and $b$ respectively denote electromagnetic fields within and without the boundary, $\hat{\mathbf{n}}$ denotes the outward pointing normal, while $J_s$ and $M_s$ denote electric and magnetic surface currents along the boundary.

metasurfaces and non-planar metasurfaces remains largely unexplored.

In this paper we report our progress in investigating wavefront generation using an active and non-planar metasurface. We call our metasurface an active closed Huygens' surface: as a Huygens' surface it contains electric and magnetic responses which are spatially orthogonal to one another; as a closed surface it geometrically wraps around an area of interest within which an arbitrary field distribution can be generated.

## II. FORMULATION AND DESIGN

### A. Conceptual Overview: A Closed Huygens' Surface

Fig. 1 depicts electromagnetic fields inside and outside a fictitious closed surface which supports the flow of electric and magnetic currents. The equivalence principle of electromagnetics states that the electromagnetic effect of sources within an enclosed boundary can be replicated by fictitious electric and magnetic currents tangential to the boundary [20]. These electric and magnetic currents are in turn related to the fields at the boundary through:

$$\mathbf{J_s} = \hat{\mathbf{n}} \times (\mathbf{H_b} - \mathbf{H_a}) \tag{1}$$

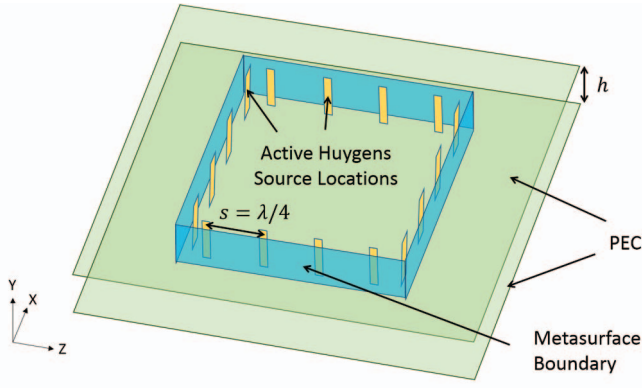$$\mathbf{M_s} = -\hat{\mathbf{n}} \times (\mathbf{E_b} - \mathbf{E_a}), \tag{2}$$

Fig. 2. A diagram depicting the layout of the effective 2D environment, within which the active closed Huygens' surface is studied.
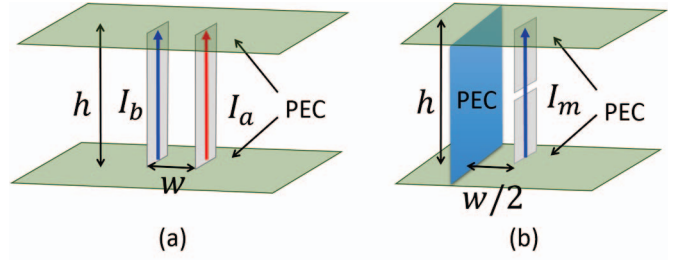


Fig. 3. A diagram showing the active Huygens' source. (a) A twin current active Huygens' source as reported in [21]. (b) A further simplified Huygens' source which has been adopted for the present work.

where $\mathbf{J_s}$ and $\mathbf{M_s}$ represent respectively the electric and magnetic currents at the boundary surface, the subscripts $a$ and $b$ denote respectively regions within and without the closed Huygens' surface, and $\hat{\mathbf{n}}$ is the outward-pointing normal.

From (1) and (2) one can deduce that, if sources from either region $a$ or $b$ are removed, such that the field vanishes in that region, one can retain the same field in the other region, by appropriately compensating the electric and magnetic currents along the boundary. This can be achieved by placing an active Huygens' surface along the boundary, which injects the required currents across the surface to produce corresponding electromagnetic waveforms. In this manner, the active closed Huygens' surface can be employed to generate an arbitrary waveform within a selective region, including waveforms which would otherwise require unrealistic or hard to arrange sources (such as sources from infinity).

### B. 2D Formulation

For simplicity we study wavefront generation with a closed Huygens' surface in a 2D environment, as shown in Fig. 2. We experimentally facilitate this environment within a parallel-plate waveguide (formed by two parallel perfect electric conductor (PEC) plates) with height of $h << \lambda/2$, which renders all electromagnetic field components invariant in the $y$-direction and restricts the polarization to $TE_Y$ (i.e. $(E_x, E_z, H_y) = 0$). Within this waveguide, we define as our boundary a square of sides $1\lambda$ in both $x$- and $z$-directions. To create the active Huygens' surface along this boundary, we place 16 Huygens' source elements at intervals of $s = \lambda/4$ along this boundary, in the manner shown in Fig. 2.

### C. Huygens' Source Element

In previous works [21], [22] we proposed two different elements which suffice as a Huygens' source in a 2D environment. The more general approach we reported in [21] is shown in Fig. 3a. This active Huygens' source includes two current wires,

$$I_a = 0.5I_e + I_m \tag{3}$$

$$I_b = 0.5I_e - I_m \tag{4}$$

Here $I_e$ and $I_m$ are current dipole and current loop components which respectively relate to the electric and magnetic surfaces currents through:

$$\mathbf{J_s} = \mathbf{I_e}/s \tag{5}$$

$$\mathbf{M_s} = -\hat{\mathbf{n}} \times \frac{j\omega\mu\mathbf{I_m}w}{s}. \tag{6}$$

Here $\mathbf{I_e}$ and $\mathbf{I_m}$ denote vectorial current quantities pointing in the $+y$-direction as depicted in Fig. 3. $\hat{\mathbf{n}}$ denotes the outward pointing normal and $h$, $w$ and $s$ respectively denote the waveguide height, the width of the current loop and the separation between adjacent Huygens' source elements (see Figs. 2 and 3a). Essentially, this element generates (i) an effective electric current through co-propagating currents in wires $a$ and $b$, and (ii) an effective magnetic current through counter-propagating currents in wires $a$ and $b$, which form a current loop when "connected" through the waveguide's top and bottom plates.

While this active Huygens' source suffices for many applications, we further simplify this by (i) shorting out the effective electric current with a metallic back wall, and (ii) replacing the current wire with an electric dipole, which leads to a more practical implementation. Fig. 3b shows the resulting active Huygens' source element we have adopted for simulation and experimentation in the present work. We emphasize that in this derivation, excitation to the electric dipole follows the current weight of the magnetic current $I_m$, *not* its electric counterpart.

### III. SIMULATION

With 16 dipole antennas, placed $\lambda/4$ apart, $\lambda/20$ away from metallic side walls and within a parallel-plate waveguide of height 38.1 mm we simulate wavefront generation at the frequency of 1 GHz (i.e. $\lambda = 300$ mm).

For a specific waveform, we find the appropriate Huygens' source currents by requiring that all electromagnetic field components vanish outside the boundary. With this condition, (1) and (2) can be rewritten as

$$\mathbf{J_s} = -\hat{\mathbf{n}} \times \mathbf{H} \tag{7}$$

$$\mathbf{M_s} = \hat{\mathbf{n}} \times \mathbf{E}, \tag{8}$$

Fig. 5. A signal flow diagram for the experimental apparatus. Dashed lines indicate command path. Dash-dot lines indicate DC bias or DC power lines. Solid lines denote RF signal flow.
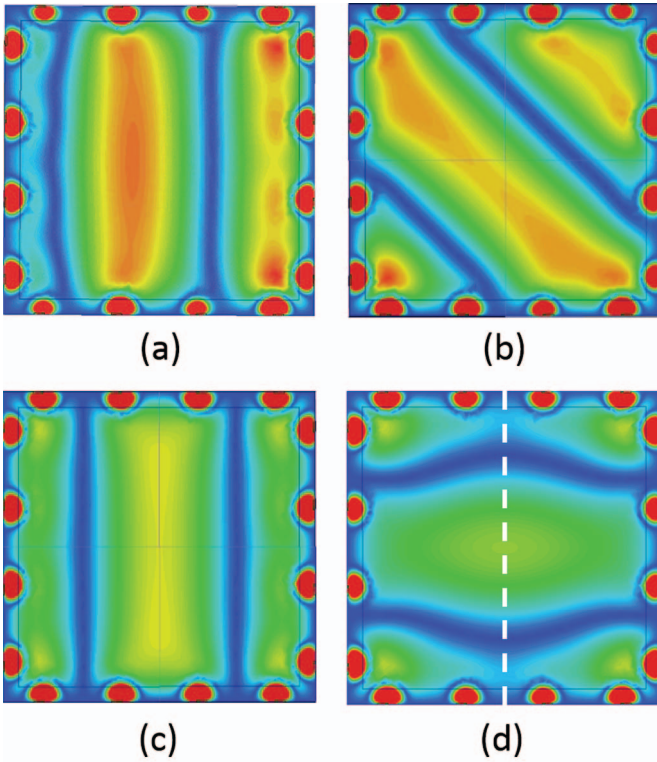
Fig. 4. Full-wave simulation results for wavefront generation using the active closed Huygens' surface. The generated waveforms are (a) a travelling waveform in the $z$-direction; (b) a travelling wave in a diagonal direction, $45°$ from the $x$-axis; (c) a standing wave in the $x$-direction, with electric field maxima very close to the metallic side walls and (d) a superoscillation wave with a sub-wavelength focus at the image plane $z = 0$ (denoted by the white dashed line). For subfigures (a) and (b) the real part of the electric field phasor is plotted; for subfigures (c) and (d) the electric field phasor amplitude is plotted.

which relate the desired electromagnetic fields at the Huygens' surface boundary with currents from which they can be generated. In particular, equation (8) will be used along with (6) to find the current excitation on the dipoles. In full rigor, the synthesis of the desired wavefront requires a continuous current distribution across the boundary contour, which in most cases would prove impractical. Notwithstanding, when we place our Huygens' sources at a separation distance below half-wavelength, the Nyquist criterion ensures that we can faithfully synthesize the target waveform away from the evanescent near-field of the Huygens' source elements.

To numerically verify the synthesis of arbitrary waveforms within the cavity, we perform full-wave simulations using the commercial software Ansys HFSS. This software solves Maxwell's equations in a user-defined environment using the finite element method. In doing so it finds the electromagnetic fields within the cavity which would arise as a result of the driven dipole sources.

Fig. 4 shows four desired waveforms that we have generated in simulation: (a) a travelling waveform in the $z$-direction; (b) a travelling wave in a diagonal direction, $45°$ from the $x$-axis; (c) a standing wave in the $x$-direction, with electric field maxima very close to the metallic side walls and (d) a superoscillation wave with a sub-wavelength focus at the
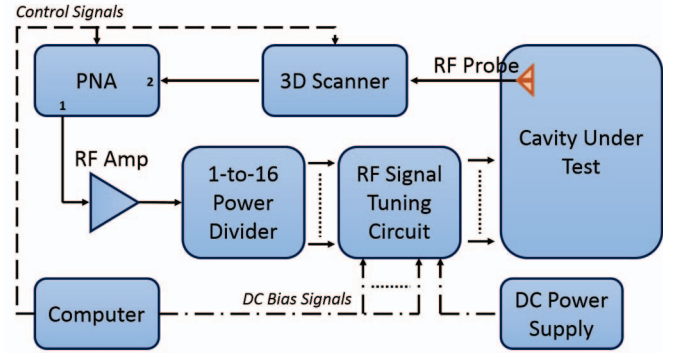
image plane $z = 0$. All these waveforms are unconventional, in that they cannot be formed by a linear combination of modes for the simulation environment (a rectangular cavity surrounded by metallic walls). Particularly, the generation of the superoscillation waveform within the confines of the cavity avoids unwanted high-energy regions of the waveform, and hence leads to dramatic energy savings and avoids potential challenges with sensitivity [22]–[25]. Fig. 4 shows indeed the faithful generation of all designed waveforms. Aside from areas of very close proximity to individual Huygens' source elements, all designed waveforms are almost almost exactly synthesized.

## IV. PROGRESS IN EXPERIMENTAL DEMONSTRATION

We are in the process of demonstrating waveform synthesis using an active closed Huygens' surface. Fig. 5 shows a schematic of the experimental apparatus; fig. 6 shows photographs of parts of the experimental apparatus. The experiment is facilitated by an Agilent programmable network analyzer (PNA). The PNA's transmitting port sends a 1 GHz signal through a power amplifier and into a 16-way power divider. The output channels from the power divider are fed, in parallel fashion, into a 16-channel RF signal tuner board. This board introduces a voltage-controlled attenuation and phase shift to each RF channel. As one alters the bias voltage for the attenuator and phase-shifters for each channel, the amplitude and phase of each RF channel can be independently tuned. We designed and assembled the RF tuner in-house; post-assembly testing shows proper operation of all RF channels, with an $S_{21}$ amplitude tunability of about 20dB and a phase range of $360°$. This tuning range enables the synthesis of many waveforms including the ones simulated in the previous subsection.

The RF signals are tuned to achieve the proper signal weighting for the dipole feed current $I_m$ for each Huygens' source element. Thereafter, these signals are fed to their corresponding Huygens' source elements within the PEC cavity. We constructed the cavity using metallic side walls, sandwiched between two perforated metallic plates. The perforation (a hexagonal arrangement of holes) does not alter the field within the cavity since the center-to-center distance between adjacent holes, at 9.525 mm, is significantly sub-wavelength. Perforation at the top plate allows for the penetration of a monopole probe, which detects the electric field as a function of location
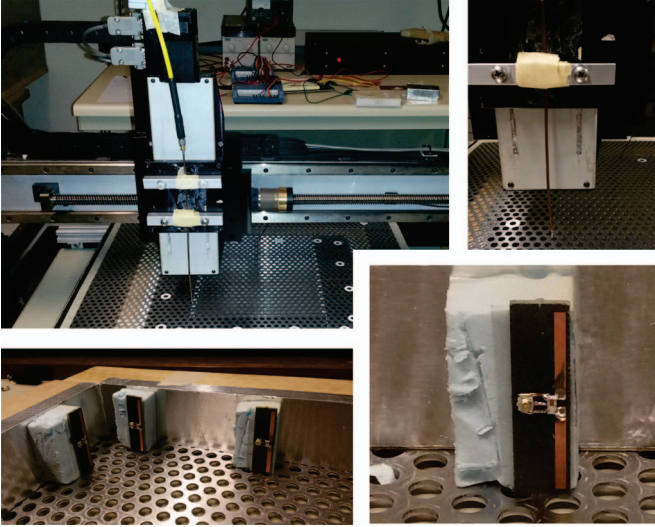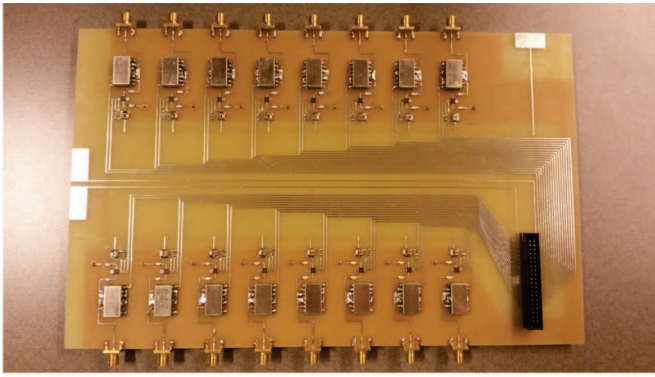
Fig. 6. Photographs of parts of the experimental apparatus. Top: The RF Signal Tuning Circuit. Middle Left: The cavity resting beneath the XYZ scanner, with the probe station in the foreground and the signal feeding electronics in the background. Middle Right: A close-up of the RF probe. Lower Left: A photo of a few Huygens' source dipoles, seen when one removes the top plate of the cavity. Lower Right: A Close-up of an individual dipole circuit.



Fig. 7. Experimental validation of the cavity measurement setup. (a) Simulated the electric field profile ($|\mathbf{E}|$) for the single-dipole excitation scenario. The white box indicates the area accessible to the scanner in the experiment. (b) Experimental measurement of normalized $S_{21}$ across the cavity.

We introduced a simple active Huygens' source and used it to build an active Huygens' surface in an effective 2D environment. Full-wave simulations confirm the faithful generation of arbitrary waveforms within a rectangular cavity, including the generation of "modes" which would not normally exist within the cavity, and a superoscillation waveform which features a sub-wavelength spot size without sidebands. Early experimental results are encouraging: a single dipole measurement matches very well with simulation results. The active closed Huygens' source represents a systematic way to synthesize an arbitrary waveform in a selected region, with wide-ranging applications in medical imaging and therapy, super-resolution imaging, power concentration and electromagnetic testing.

within the cavity, then transmits the collected voltage signal to the receive port of the PNA. A mechanical scanner, controlled by in-house measurement software, scans the probe across the cavity through the top plate perforations. At each point the PNA measures the $S_{21}$ at 1 GHz, which is proportional to the electric field strength at the particular location.

Currently we have verified the operation of our experimental setup with a single dipole radiation. In this characterization experiment, the output of the power amplifier connects directly to one Huygens' source element within the cavity. No current is fed to other dipole ports. The resultant scan is produced in Fig. 7 alongside the simulation result for the corresponding scenario. The excellent agreement between measurement and simulation verifies the functional operation of the experimental setup. In the near future, we aim to report a full experimental demonstration of the unconventional cavity waveforms shown in Fig. 4.

## V. Conclusion

In this paper we have reported our investigation on generating arbitrary waveforms with active closed Huygens' surfaces.
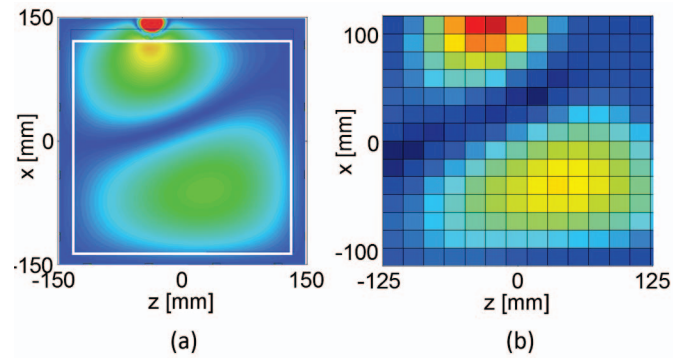
## References

[1] J. B. Pendry, "Negative refraction makes a perfect lens," *Phys. Rev. Lett.*, vol. 85, no. 18, pp. 3966–3969, Apr 2000.

[2] G. V. Eleftheriades, A. K. Iyer, and P. C. Kremer, "Planar negative refractive index media using periodically l-c loaded transmission lines," *IEEE Trans. Microw. Theory Techn.*, vol. 50, no. 12, pp. 2702–2712, Dec 2002.

[3] C. L. Holloway, M. A. Mohamed, E. F. Kuester, and A. Dienstfrey, "Reflection and transmission properties of a metafilm: with an application to controllable surface composed of resonant particles," *IEEE Trans. Electromagn. Compat.*, vol. 47, no. 4, pp. 853–865, Nov 2005.

[4] G. V. Eleftheriades and A. M. H. Wong, "Holographic screens for sub-wavelength focusing in the near-field," *IEEE Microwave and Wireless Components Letters*, vol. 18, no. 4, pp. 236–238, Apr 2008.

[5] L. Markley, A. M. H. Wong, Y. Wang, and G. V. Eleftheriades, "Spatially shifted beam approach to subwavelength focusing," *Phys. Rev. Lett.*, vol. 101, no. 11, p. 113901, Sep 2008.

[6] A. Grbic, L. Jiang, and R. Merlin, "Near-field plates: Subdiffraction focusing with patterned surfaces," *Science*, vol. 320, no. 5875, pp. 511–513, Apr 2008.

[7] M. Selvanayagam and G. V. Eleftheriades, "Circuit modeling of huygens surfaces," *IEEE Antennas Wireless Propag. Lett.*, vol. 12, pp. 1642–1645, Dec 2013.

[8] J. P. S. Wong, M. Selvanayagam, and G. V. Eleftheriades, "Design of unit cells and demonstration of methods for synthesizing Huygens metasurfaces," *Photonic. Nanostruct. Fundam. Appl.*, vol. 12, no. 4, pp. 360–375, Aug. 2014.

[9] ——, "Polarization considerations for scalar huygens metasurfaces and characterization for 2-d refraction," *IEEE Trans. Microw. Theory Techn.*, vol. 63, no. 3, pp. 913–924, Mar. 2015.

[10] C. Pfeiffer and A. Grbic, "Metamaterial Huygens' surfaces: tailoring wave fronts with reflectionless sheets," *Phys. Rev. Lett.*, vol. 110, no. 19, p. 197401, May 2013.

[11] F. Monticone, N. M. Estakhri, and A. Alù, "Full control of nanoscale optical transmission with a composite metascreen," *Phys. Rev. Lett.*, vol. 110, no. 20, p. 203903, May 2013.

[12] A. Alù and N. Engheta, "Full control of nanoscale optical transmission with a composit metascreen," *Phys. Rev. Lett.*, vol. 100, no. 11, p. 113901, Mar 2008.

[13] Y. Wang, A. M. H. Wong, L. Markley, A. S. Helmy, and G. V. Eleftheriades, "Plasmonic meta-screen for alleviating the trade-offs in the near-field optics," *Opt. Express*, vol. 17, no. 15, pp. 12 351–12 361, Jul 2009.

[14] N. Yu, P. Genevet, M. A. Kats., F. Aieta, J. Tetienne, F. Capasso, and Z. Gaburro, "Light propagation with phase discontinuities: generalized laws of reflection and refraction," *Science*, vol. 334, pp. 333–337, Oct. 2011.

[15] X. Ni, N. K. Emani, A. V. Kildishev, A. Boltasseva, and V. M. Shalaev, "Broadband light bending with plasmonic nanoantennas," *Science*, vol. 335, p. 427, Jan 2012.

[16] I. Staude, A. E. Miroshnichenko, M. Decker, N. T. Fofang, S. Liu., E. Gonzales, J. Dominguez, T. S. Luk, D. N. Neshev, I. Brener, and Y. Kivshar, "Tailoring directional scattering through magnetic and electric resonances in subwavelength silicon nanodisks," *ACS Nano*, vol. 7, no. 9, pp. 7824–7832, Aug 2013.

[17] M. Kim, A. M. H. Wong, and G. V. Eleftheriades, "Optical huygens' metasurfaces with independent control of the magnitude and phase of the local reflection coefficients," *Phys. Rev. X*, vol. 4, p. 041042, Dec 2014. [Online]. Available: http://link.aps.org/doi/10.1103/PhysRevX.4.041042

[18] D. Lin, P. Fan, E. Hasman, and M. L. Brongersma, "Dielectric gradient metasurface optical elements," *Science*, vol. 345, pp. 298–302, Jul 2014.

[19] C. Pfeiffer, N. K. Emani., M. K. Shaltout, A. Boltasseva, V. M. Shalaev, and A. Grbic, "Efficient light bending with isotropic metamaterial huygens' surfaces," *Nano Lett.*, vol. 14, no. 5, pp. 2491–2497, Apr 2014.

[20] R. F. Harrington, *Time-harmonic electromagnetic fields*, ser. IEEE Pass Series on Electromagnetic Wave Theory, D. G. Dudley, Ed. IEEE Press, 2001.

[21] A. M. H. Wong and G. V. Eleftheriades, "A simple active huygens source for studying waveform synthesis with huygens metasurfaces and antenna arrays," *IEEE International Symposium on Antennas and Propagation*, Jul. 2015.

[22] ——, "Superoscillations without sidebands: power efficient sub-diffraction imaging with propagating waves," *Sci. Rep.*, vol. 5, no. 8449, Feb 2015.

[23] P. J. S. G. Ferreira and A. Kempf, "Superoscillations: faster than the nyquist rate," *IEEE Trans. Signal Process.*, vol. 54, no. 10, pp. 3732–3740, Oct 2006.

[24] A. M. H. Wong and G. V. Eleftheriades, "Adaptation of schelkunoff's superdirective antenna theory for the realization of superoscillatory antenna arrays," *IEEE Antennas Wireless Propag. Lett.*, vol. 9, pp. 315–318, Apr 2010.

[25] ——, "An optical super-microscope for far-field, real-time imaging beyond the diffraction limit," *Sci. Rep.*, vol. 3, p. 1715, 2013.